Heat-constrained modelling of calcium sulphate reduction

by L.A. Jordan[1] and D. van Vuuren[1]

Affiliation:
[1]Department of Chemical Engineering, University of Pretoria, South Africa.

Correspondence to:
L.A. Jordan

Email:
luke.jordan.up@gmail.com

Dates:
Received: 22 Jun. 2021
Revised: 30 Jun. 2022
Accepted: 28 Jul. 2022
Published: October 2022

How to cite:
Jordan, L.A, and van Vuuren, D. 2022 Heat-constrained modelling of calcium sulphate reduction. Journal of the Southern African Institute of Mining and Metallurgy, vol. 122, no. 10, pp. 607–616

DOI ID:
http://dx.doi.org/10.17159/2411-9717/1530/2022

ORCID:
L.A. Jordan
https://orcid.org/0000-0001-9116-7073

Synopsis

A two-dimensional finite difference model has been developed to describe the reduction of kilogram quantities of dehydrated phosphogypsum. The model's scope has been limited to focus on the heat transfer and reactions that occur within a mass of material contained in a vessel inside a furnace rather than also including the effects of heat transfer to the vessel. Changes in the heat transfer properties (k, ρ, and C_p) are incorporated as the composition of the mass changes as the chemical reactions progress.

The model is validated against experimental data, with samples heated to 1000°C at 3°C min^{-1} while purging with nitrogen gas. A sensitivity analysis of model predictions to the pre-exponential factor of the reaction rate constant of the main chemical reaction and the thermal conductivity of the powder bed indicated that, at the envisaged process conditions, the behaviour of the system depends much more on the rate of heat transfer than on the rate of the chemical reaction. The model demonstrated a significant increase in accuracy when the thermal conductivity was modelled to increase linearly with temperature compared to assuming a constant value.

Keywords

carbothermal reduction; phosphogypsum; modelling; waste treatment.

Introduction

Millions of tons of phosphogypsum- and gypsum-rich solid wastes and sludge are generated by the chemical manufacturing industry and the industrial waste remediation sector. Phosphogypsum is a by-product of the production of phosphoric acid whereas gypsum is a by-product of many other processes, including the production of hydrofluoric, citric, and boric acids, treatment of waste from desulphurization of flue gases from coal-fired power stations, ore smelting, and acid mine water treatment. Although gypsum is widely used in the construction industry, phosphogypsum is generally regarded as unsuitable for further use, and is stored indefinitely in large stockpiles. These stacks constitute substantial expenses for the industry, occupying significant areas of land and being subject to increasingly stringent regulations on waste materials and their disposal. Costs associated with the transportation and storage of phosphogypsum in dumps can be as high as about 18% of the cost of phosphoric acid production, and significantly more with the transition to more reliable hydrotransport of the phosphogypsum.

An alternative approach to the often-expensive management of stockpiles is to treat the waste with the aim of converting it into potentially useful products (de Beer *et al.*, 2015; Tao *et al.*, 2001).

Gypsum waste can represent a good resource for the recovery of elemental sulphur (S) and calcium carbonate ($CaCO_3$), while in addition to this phosphogypsum can also contain rare earth elements (REEs) that could constitute a potential secondary source of these elements (Kulczycka *et al.*, 2016; Walawalkar, Nichol, and Azimi, 2016).

Sulphur is a key raw material for many manufacturing industries including the production of acids, explosives, fertilizers, insecticides, steel, and titanium dioxide (Cork, Jerger, and Maka, 1986). Cork, Jerger, and Maka (1986) also suggest sulphur's application as an alternative feedstock to produce polymeric materials. Calcium carbonate is used in a wide variety of commercial applications in two main forms, ground calcium carbonate (GCC) and precipitated calcium carbonate (PCC). GCC features in the manufacture of concrete or Portland cement, lime for use in soil stabilization and acid neutralization, water treatment, and flue gas desulphurization (Oates, 1986). PCC sees extensive use as a filler and tre coating pigment in paper, plastics, paints, rubbers, and adhesives (Windholz, 1983; Zhang *et al.*, 2010a).

REEs have many uses due to their physical and chemical characteristics, which include magnetism, luminescence, conductivity, electro-optical, and nuclear properties (Akah, 2017). Rare earths have contributed to the improvement of the operating efficiency, longevity, miniaturization of components,

and to the complexity and footprint of many industrial, military and aerospace instruments. REE use is further growing as the development of new applications and expansion of current rare earth consumer industries continues (Dutta *et al.*, 2016).

The recovery of sulphur, calcium carbonate, and REEs from gypsum entails *inter alia* carbothermal reduction of the gypsum to form a sulphide salt that can then be converted into forms that are saleable (van Vuuren and Maree, 2018). It has been suggested that a continuously operated tunnel kiln might be the best type of reactor to use for the carbothermal reduction step, but sufficient information is currently not available to design and construct such a kiln with confidence.

Literature survey

Calcium sulphate waste

Nengovhela *et al.* (2007) proposed a multi step - process for the recovery of sulphur and $CaCO_3$ from gypsum waste. It involves the three following steps:

- Thermal reduction (850–1100°C) of $CaSO_4$ to produce calcium sulphide (CaS) using a reducing agent (*e.g.* solid carbonaceous materials such as coal or activated carbon (Equation [1]), or a reducing gas such as carbon monoxide or hydrogen)

$$CaSO_4(s) + 2C(s) \rightarrow CaS(s) + 2CO_2(g) \quad [1]$$

- Direct aqueous carbonation of CaS to produce hydrogen sulphide (H_2S) and $CaCO_3$

$$CaS(s) + H_2O(l) + CO_2(g) \rightarrow H_2S(g) + CaCO_3(s) \quad [2]$$

- Sulphur is produced from H_2S via the commercially available Clauss process (Mark *et al.*, 1978):

$$4H_2S(g) + 3O_2(g) \rightarrow 2SO_2(g) + 2H_2O(g) \quad [3]$$

$$4H_2S(g) + 2SO_2(g) \rightarrow 3S_2(g) + 4H_2O(g) \quad [4]$$

Although each of these steps has been subjected to a number of studies to develop understanding (de Beer *et al.*, 2014; Brooks and Lynn, 1997; Kato, Murakami, and Sugawara 2012; Ma *et al.*, 2011; Miao *et al.*, 2012; Ning *et al.*, 2011; Ruto *et al.*, 2011; Selim, Gupta, and Al Shoaibi, 2013; Zhang *et al.*, 2010b) and propose alternatives (de Beer *et al.*, 2015; Sliger, 1988), process step 1 is the step of interest. The reduction of the sulphate is straightforward, but not without complications. A secondary reaction, given by

$$3CaSO_4(s) + CaS(s) \rightarrow 4CaO(s) + 4SO_2(g) \quad [5]$$

can also occur (initiating at 900°C); however, as this is an oxidative reaction, sufficient excess carbonaceous material serves to mitigate the reaction's impact (Mbhele *et al.*, 2009; Strydom, Groenewald, and Potgieter, 1997a).

Typically, the reduction to CaS is carried out in a rotary kiln, using charcoal and gypsum as the sources of carbon and sulphate, respectively (Li and Zhuang, 1999).

Several authors have reported that the thermal reduction process occurs via a gaseous intermediate, and can mostly likely be described by (Gorkan *et al.*, 2000; Oh and Wheelock, 1990):

$$CaSO_4(s) + 4CO(g) \rightarrow CaS(s) + 4CO_2(g) \quad [6]$$

To this end, it has also been found that the presence of O_2 and CO_2 is undesirable as they favour the formation of calcium oxide and calcium sulphate. Thus, as reported by Jagtap, Pande, and Gokarn (1990), to effectively favour the formation of CaS from $CaSO_4$ an excess of carbon monoxide (if using a gaseous reducing agent) should be present in the kiln; alternatively, if a solid reducing agent is used, an environment that favours excess amounts of CO in the kiln is desirable (Motaung *et al.*, 2015).

As reported by Yan *et al.* (2014) and corroborated by Mbhele *et al.* (2009) and Motaung et al. (2015), temperature plays an important role in the conversion of the sulphate, with increasing temperature yielding an increased reaction ratewith.

Mbhele *et al.* (2009), who focused on the recovery of sulphur from waste gypsum using activated carbon, investigated several process conditions to determine their impact on the yield of CaS and subsequently sulphur. Naturally, a longer reaction time yielded greater conversions, with sufficient residence time being 20 minutes for a sample of approximately 180 g. It was also found that CaO production (as per Equation [5]) was favoured at low carbon to gypsum ratios, and CaS becomes favoured at carbon to gypsum ratios greater than 2, with higher yields as the carbon content increases. Furthermore, it was found that as the average particle size of the mixture decreases, improved conversions can be achieved. Lastly, Mbhele *et al.* (2009) estimated that from 1 t of pure gypsum, 0.18 t of sulphur and 0.58 t of $CaCO_3$ could be recovered.

Although numerous authors have looked at catalytic effects, making use of catalysts such as ferric oxide (Strydom, Groenewald, and Potgieter, 1997b), potassium dichromate (Kale, Pande, and Gokam, 1992), semi-coke additives (Trikkel and Kuusik, 1994), stannous sulphate and vanadium pentoxide (Zadick, Zavaleta, and McCandless, 1972) to achieve increased yields and lower initiation temperatures, this is not applicable to the current study but is worth noting. Furthermore, as the typical choice of kiln to perform the reduction in is a rotary kiln, several authors have also reported the effects of pelletization and binder choice (Finney, Sharifi, and Swithenbank, 2009; Motaung *et al.*, 2015; Nengovhela *et al.*, 2007).

Theory

Crucible model

The scope of the model has been limited to focus on the heat transfer within the reacting material contained in the furnace, rather than describing the entire furnace and all the conductive, convective, and radiant heat transfer processes involved. Additionally, the feed of interest has also been limited to a mixture of dehydrated phosphogypsum and coal. The Python language was used in the simulation of the system to solve the relevant finite-difference equations and discretized kinetics.

Internal heat transfer

Heat transfer is modelled using a two-dimensional finite difference approach – in the radial direction of a symmetric slice of the crucible. Çengel and Ghajar (2015) and Welty, Wicks, and Wilson (1969) describe the formulation of the transient model, beginning with the energy balance on a volume element as

$$\Delta t \times \sum_{\text{All sides}} \dot{Q} + \Delta t \times \dot{e}_{\text{element}} = \Delta E_{\text{element}} \quad [7]$$

where the rate of heat transfer, $\dot{Q}\,(W)$, consists of conduction terms for the neighbouring nodes, and ΔE and $\dot{e}$ represent the energy content (J) and heat generated from reaction (J) terms for an element, respectively. Noting that $\Delta E_{element}=\rho C_p \Delta T$, the

derivation with respect to the r and z directions and time is

$$\frac{1}{r}\frac{\partial}{\partial r}\left(kr\frac{\partial T}{\partial r}\right)+\frac{\partial}{\partial r}\left(k\frac{\partial T}{\partial z}\right)+\dot{e}_{\text{element}}=\rho C_p\left(\frac{\partial T}{\partial t}\right) \quad [8]$$

which, after dividing throughout with k and simplification (noting that $\alpha = k/\rho C_p$)

$$\frac{\partial^2 T}{\partial r^2}+\frac{1}{r}\left(\frac{\partial T}{\partial r}\right)+\frac{\partial^2 T}{\partial z^2}+\frac{\dot{e}_{\text{element}}}{k}=\frac{1}{\alpha}\left(\frac{\partial T}{\partial t}\right) \quad [9]$$

Using the finite-difference method to approximate the partial derivatives, and noting that the volume element centred around a general interior node (m,n) involves conduction from four sides (right, left, top, and bottom), this then yields

$$\begin{aligned}\frac{T^i_{m-1,n}-2T^i_{m,n}+T^i_{m+1,n}}{\Delta r^2}+\frac{1}{r}\left(\frac{T^i_{m+1,n}-T^i_{m-1,n}}{2\Delta r}\right)\\ +\frac{T^i_{m,n-1}-2T^i_{m,n}+T^i_{m,n+1}}{\Delta z^2}+\frac{\dot{e}_{m,n}}{k}\\ =\frac{1}{\alpha}\left(\frac{T^{i+1}_{m,n}-T^i_{m,n}}{\Delta t}\right)\end{aligned} \quad [10]$$

Taking a square mesh ($\Delta r = \Delta z = l$) and multiplying throughout by $\alpha\Delta t$

$$\begin{aligned}\frac{\alpha\Delta t}{l^2}\left(T^i_{m-1,n}+T^i_{m,n-1}-4T^i_{m,n}+T^i_{m+1,n}+T^i_{m,n+1}\right)\\ +\frac{\alpha\Delta t}{2rl}\left(T^i_{m+1,n}-T^i_{m-1,n}\right)+\frac{\alpha\Delta t}{k}\dot{e}_{m,n}\\ =T^{i+1}_{m,n}-T^i_{m,n}\end{aligned} \quad [11]$$

And utilizing the mesh Fourier number, $\tau = \alpha\Delta t/l^2$, for the final transformation then gives

$$\begin{aligned}T^{i+1}_{\text{m,n}}=\tau\left(T^i_{m-1,n}+T^i_{m,n-1}+T^i_{m+1,n}+T^i_{m,n+1}\right)\\ +(1-4\tau)T^i_{m,n}+\frac{\tau l}{2r}\left(T^i_{m+1,n}-T^i_{m-1,n}\right)\\ +\tau\frac{e^i_{m,n}l^2}{k}\end{aligned} \quad [12]$$

Which, rewriting in a simpler-to-read form, yields the explicit formulation for an internal node:

$$\begin{aligned}T^{i+1}_{\text{node}}=\tau\left(T^i_{\text{left}}+T^i_{\text{bottom}}+T^i_{\text{top}}+T^i_{\text{right}}\right)+(1-4\tau)T^i_{\text{node}}\\ +\frac{\tau l}{2r}\left(T^i_{\text{right}}-T^i_{\text{left}}\right)+\tau\frac{e^i_{node}l^2}{k}\end{aligned} \quad [13]$$

To satisfy the insulated and zero-temperature-gradient boundary conditions, the boundary nodes are treated as internal nodes with an additional fictional node set equal to the node preceding the boundary, as demonstrated in Figure 1.

However, as r approaches zero, an accommodation is required,

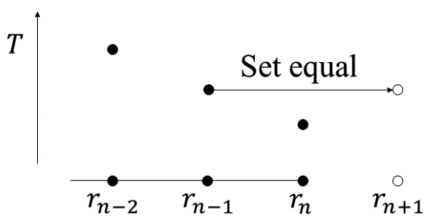

Figure 1—Illustration of an insulated boundary condition with a fictional node r_{n+1} (or z_{m+1}) with $T_{n+1} = T_{n-1}$

which can be achieved by applying the limit as r approaches zero of Equation [9] as

$$\lim_{r\to 0}\left[\frac{\partial^2 T}{\partial r^2}+\frac{1}{r}\left(\frac{\partial T}{\partial r}\right)+\frac{\partial^2 T}{\partial z^2}+\frac{\dot{e}_{element}}{k}\right]=\lim_{r\to 0}\left[\frac{1}{\alpha}\left(\frac{\partial T}{\partial t}\right)\right] \quad [14]$$

The only term affected by the limit, $\frac{1}{r}\left(\frac{\partial T}{\partial r}\right)$, requires application of L'Hopitals rule. Thus, the equation for the side boundary condition (following the same transformations as above) is

$$2\frac{\partial^2 T}{\partial r^2}+\frac{\partial^2 T}{\partial z^2}+\frac{\dot{e}_{\text{element}}}{k}=\frac{1}{\alpha}\left(\frac{\partial T}{\partial t}\right) \quad [15]$$

$$\begin{aligned}\frac{2T^i_{m-1,n}-4T^i_{m,n}+2T^i_{m+1,n}}{\Delta r^2}+\frac{T^i_{m,n-1}-2T^i_{m,n}+T^i_{m,n+1}}{\Delta z^2}\\ +\frac{\dot{e}_{m,n}}{k}=\frac{1}{\alpha}\left(\frac{T^{i+1}_{m,n}-T^i_{m,n}}{\Delta t}\right)\end{aligned} \quad [16]$$

Rewritten in a simpler-to-read form, the explicit formulation for the side boundary node is given by

$$\begin{aligned}T^{i+1}_{\text{node}}=\tau\left(2T^i_{\text{left}}+T^i_{\text{bottom}}+T^i_{\text{top}}+2T^i_{\text{right}}\right)\\ +(1-6\tau)T^i_{\text{node}}+\tau\frac{\dot{e}^i_{node}l^2}{k}\end{aligned} \quad [17]$$

Reaction kinetics

The reaction and conversion of species present is described by the kinetic model proposed by Kato, Murakami, and Sugawara (2012). It is suggested that the reaction proceeds as follows:

$$CaSO_4 + 2C \rightarrow CaS + 2CO_2 \quad [18]$$

$$3CaSO_4 + CaS \rightarrow 4CaO + 4SO_2 \quad [19]$$

and, assuming that each rate can be expressed as a first-order reaction with respect to $CaSO_4$, CaS, and/or C concentrations in the solid phase, the mass balances for the components are given by

$$\frac{\text{d}[CaSO_4]}{\text{d}t}=-k_1[CaSO_4][C]-3k_2[CaSO_4][CaS] \quad [20]$$

$$\frac{\text{d}[CaS]}{\text{d}t}=k_1[CaSO_4][C]-k_2[CaSO_4][CaS] \quad [21]$$

$$\frac{\text{d}[CaO]}{\text{d}t}=4k_2[CaSO_4][CaS] \quad [22]$$

$$\frac{\text{d}[C]}{\text{d}t}=-2k_2[CaSO_4][C] \quad [23]$$

The rate constants, k_1 and k_2, can be expressed using the Arhennius equation

$$k_i = k_{i(0)}\exp\left(-\frac{E_i}{RT}\right) \quad [24]$$

where the kinetic parameters (pre-exponential factor and activation energy) reported by Kato, Murakami, and Sugawara (2012) for a heating rate of 10°C min^{-1} are $k_{1(0)}$ =3.2 × 10^{15} mol^{-1} s^{-1}, E_1 = 370 kJ mol^{-1}, $k_{2(0)}$ = 1.6×10^{15} mol^{-1} s^{-1}, and E_2=400 kJ mol^{-1} respectively.

Model assumptions and procedure

Several assumptions have been made for the modelling process for the first instance of the model, and are as follows:

- The reaction species form a perfect, uniformly distributed mixture.
- Heat generation ($\dot{e}^{i}_{node}$) is given as a constant heat of reaction at 1000°C of 153.43 kJ/mol (Roine, 2018) (as the heat of reaction at 800°C is only 4.8% larger)
- Exterior boundary (top and side) temperatures are ramped from ambient according to the given heating rate, each iteration
- Concentrations of reaction species are determined using the discretized kinetics, for each node individually
- The thermal conductivity (k) of the mixture is calculated using a volume-fraction based average of the initial amounts of dehydrated phosphogypsum and coal charged and kept constant thereafter
- The heat capacity (C_p) of the mixture is calculated using a mass-fraction based average of the components present for a node at any given time
- The reacting mass does not contract
- The bulk density (ρ_B) of the mixture has been measured experimentally as 836 kg m^{-3} and is varied according to the mass loss as the reduction proceeds
- Heat transfer properties (C_p, ρ_B, α, and τ) are calculated for each node, every iteration, at the temperature of the node
- The model does not include gangue material (ash and volatiles in coal and impurities in gypsum)
- The bottom of the crucible is perfectly insulated.

As indicated by assumption 5, the thermal conductivity is a constant over the simulation, calculated using the thermal conductivity of calcium sulphate, 0.43 W m^{-1} K^{-1} (though this has been stated to range between 0.43–0.51 W m^{-1} K^{-1}) (Bejan, 2013; Green and Perry, 2008; Tesárek *et al.*, 2007) and coal, 0.26 W m^{-1} K^{-1} (Bejan, 2013; Green and Perry, 2008), and the initial volume fractions of dehydrated phosphogypsum, 0.74, and coal, 0.26. Using Equation [25], this gives a k_{mix} of 0.377 W m^{-1} K^{-1}.

Modelling is performed by initiating the system at ambient temperature and then ramping up the temperature of the exterior nodes in the finite difference mesh as per assumption 3. This simulates the external heating of the material. The finite difference equations are then used to simulate the transfer of heat into the medium, while each node also simulates the reactions occurring using the discretized kinetics to describe the changes in composition at the node, as per assumption 4. This, in turn, as per assumptions 6 and 9 above, is incorporated as a change in the heat transfer properties (C_p, and ρ_B, which affect α, and τ) used in the finite difference equations. This procedure is then iterated, continuing the ramping of the exterior nodes until equilibrium is achieved.

The heat capacity is calculated using a simple mass-fraction based (or volume-based in the case for k) average, given by

$$M_{mix} = \sum_{\text{components}} M_i \times x_i \qquad [25]$$

where M is the property in question, and x_i is the mass or volume fraction. The bulk density is varied with the mass loss caused by the reaction, assuming the volume of the reacting mass stays constant.

The model can be improved by abandoning assumption 5 and linearly varying the thermal conductivity with temperature in line with the work presented by Godbee and Ziegler (1996), Laubitz (1959), and Luikov *et al.* (1968). This is expanded in the Model Sensitivity Analysis section below.

Table I

Dehydrated phosphogypsum – major component composition (Oberholzer and Nel, 2020)

Component	Mass %
SiO_2	1.61
CaO	37
H_3PO_4	1.7605
SO_3	54.0558
Moisture	0.83
Loss on ignition	6.39

Table II

Coal proximate analysis (Oberholzer and Nel, 2020)

Component	Mass %
H_2O	2.70
Ash	16.10
Volatile matter	24.8
Fixed carbon	56.4
Total sulphur	0.453

Experimental procedure

Materials

Phosphogypsum, sourced from Foskor, which was dehydrated for 6 hours at 300°C, with an analysis as given in Table I and a heat capacity of 1380 J kg^{-1} K^{-1} (Engineering ToolBox, 2003), was used along with coal, with a proximate analysis as given in Table II and a heat capacity of 1090 J kg^{-1} K^{-1} (Engineering ToolBox, 2003).

Apparatus

Two in-house-made stainless steel crucibles were used in a medium sized muffle furnace to perform the experiments. Both three- and six-inch diameter vessels were made using 310 stainless steel, with holes drilled through the lids to allow thermocouples to be placed in various locations to capture the temperature profile of the reacting mixture. Figure 2 depicts the thermocouple layout.

Analytical Instruments

Product samples were analysed using a PANalytical X'Pert Pro powder diffractometer in σ–σ configuration with an X'Celerator detector and variable divergence- and fixed receiving slits with Fe-filtered Co-Kα radiation (λ = 1.789Å). The mineralogy was determined by selecting the best–fitting pattern from the ICSD database to the measured diffraction pattern, using X'Pert Highscore Plus software. The relative phase amounts (weight %) were estimated using the Rietveld method (X'Pert Highscore Plus). The samples were prepared according to the standardized PANalytical back-loading system, which provides nearly random distribution of the particles.

Planning

The experiments were designed around obtaining the temperature profile of the reacting mixture to adequately validate the developed model. Four experiments were performed, maintaining the heating rate (3°C min^{-1}), maximum temperature (1000°C), nitrogen purge gas flow rate (1 L min^{-1}), and reactant composition

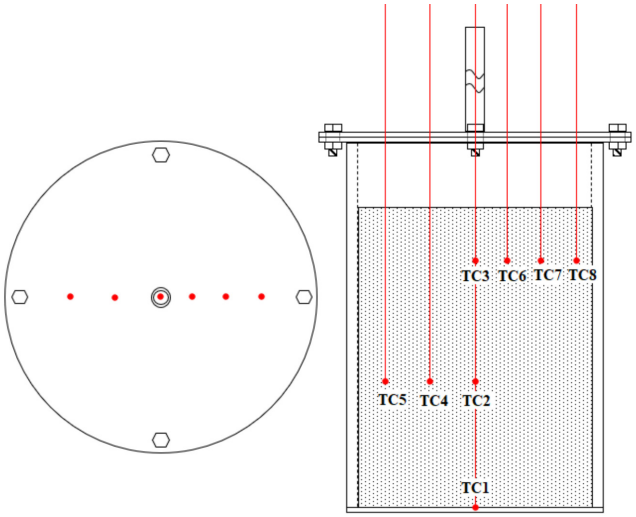

Figure 2—Thermocouple layout within crucible

Table III

Experiment description

Experiment	Crucible diameter	Mass loaded (g)
1	3 inch	350
2	3 inch	400
3	3 inch	500
4	6 inch	2000

Table IV

Thermocouple positioning

Thermocouple	3-inch crucible		6-inch crucible	
	DFC[1] (mm)	DFB[2] (mm)	DFC[1] (mm)	DFB[2] (mm)
TC1	0	0	0	0
TC2	0	70	0	70
TC3	0	120	0	120
TC4	19.4	70	33.6	70
TC5	34	70	62	70
TC6	16	120	26	120
TC7	26.6	120	47.2	120
TC8	37.8	120	68.4	120

1 Distance from centre
2 Distance from bottom

Table V

Relative phase amounts determined from XRD analysis

Experiment no.	Oldhamite (CaS) (%)	Quartz (SiO_2) (%)	Apatite (CaF) (%)	Lime (CaO) (%)
1	92.76	2.3	4.8	0.13
2	93.46	2.13	4.41	-
4	90.38	1.98	7.64	-

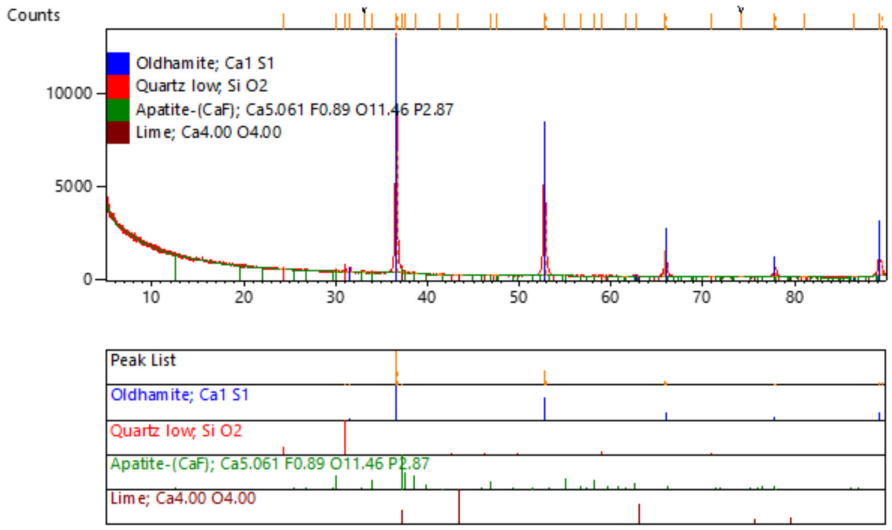

Figure 3—XRD results for a mass charge of 350 g

(mass ratio of 0.35-coal:1-$CaSO_4$ to obtain a molar ratio of 2.5-C:1-$CaSO_4$) uniformly throughout. Variances in the mass loading for the respective crucibles are detailed in Table III.

Several type-K thermocouples were placed to capture temperature profiles at various heights and radial positions as described in Table IV and graphically shown in Figure 2.

Results and discussion

Experimental results

XRD analysis suggests a very high extent of conversion with no $CaSO_4$ present in the product samples, and a CaS content varying from 90–93 wt% (Table V). Trace amounts of CaO were also detected. These findings indicate that the reaction occurred as expected, with the primary reduction to CaS dominating the side reaction producing CaO.

It should be noted that excess carbon is present in the samples; however, the peaks overlap with that of quartz, which is present as an impurity in both the phosphogypsum and coal (Figure 3).

Model validation

The model was validated by comparing the temperature profiles

Table VI

Model centre-bottom node final temperatures

Mass load (g)	Model		Experimental	
	Time to T_f (h)	T_f (°C)	Time to T_f (h)	T_f (°C)
350	10.3	1000	5.5	984
400	11.0	1000	6.48	999
500	11.9	1000	6.5	1006
2000	15.1	1000	9.78	997

of the embedded thermocouples with the equivalent predicted profiles.

The mass load in the three-inch crucible was varied to investigate whether a noticeable difference in the centre-bottom temperature profile could be seen by varying the area available for heat transfer within a constrained environment. The mass load in the six-inch crucible was kept constant and served to investigate the effect of scaling on the heat transfer. When looking at the model results presented in Table VI, although the model lags the experimental results, a general trend is present, where the additional mass causes an increase in the time required to reach 1000°C.

Considering Figure 4, as can be seen by the behaviour of TC1, TC2, TC4, and TC5 in the 350, 450, and 500 g experiments, the increase in height results in slightly delayed profiles as those nodes become more deeply embedded in the material. The packed bed in the 2000 g experiment is of similar height to the 500 g case, but with a much larger crucible diameter, subsequently the temperature profiles of the more embedded nodes are much more delayed. The intermediate plateaus of the more embedded nodes are likely due to the endothermic contribution of the heat of reaction of the more exterior nodes causing a delay or lead-time in the transfer of heat, as well as the endothermic effects within the node itself counteracting the heat transfer as the reaction proceeds.

Furthermore, Figure 4 shows that the model overestimates the time to final temperature, especially towards the centre bottom. As can be seen over the course of increasing mass, the model's degree of inaccuracy increases with increasing mass of material and vessel diameter. This suggests several possibilities: that the estimated thermal conductivity is too low, as the experimental nodes all experience faster heating than the model predicts; or that the kinetic parameters presented by Kato, Murakami, and Sugawara (2012) are not an accurate representation for the coal and gypsum used in these experiments and are under-predicting the rate of reaction.

Model sensitivity analysis

By varying the pre-exponential factor of the reaction rate constant of the $CaSO_4$ reduction reaction (k1(o) in Equation [20]) or the thermal conductivity of the system, the accuracy for the model can be evaluated and improved. As can be seen by Figure 5 (which compares the 500 g experimental case), increasing the rate of reaction does not have a pronounced effect on the model's overall accuracy, although it does decrease the time taken for a node to reach the final temperature.

The work by Godbee and Ziegler (1996), Laubitz (1959), and Luikov *et al.* (1968) on the thermal conductivity of powder beds and porous systems shows that values for k can vary between 0.2 W m^{-1} K at 25°C and 1 W m^{-1} K at 1000°C for a variety of different powders. This finding is used as a basis for the variation of the k values in the model. As can be seen in Figure 6, an increase in thermal conductivity results in a significantly closer representation of the experimental data when compared to the base case (k = 0.377) and the increased rate of reaction cases (Figure 5). This suggests that the thermal conductivity plays a more substantial role in determining the heating of the vessel than the rate of the reaction does.

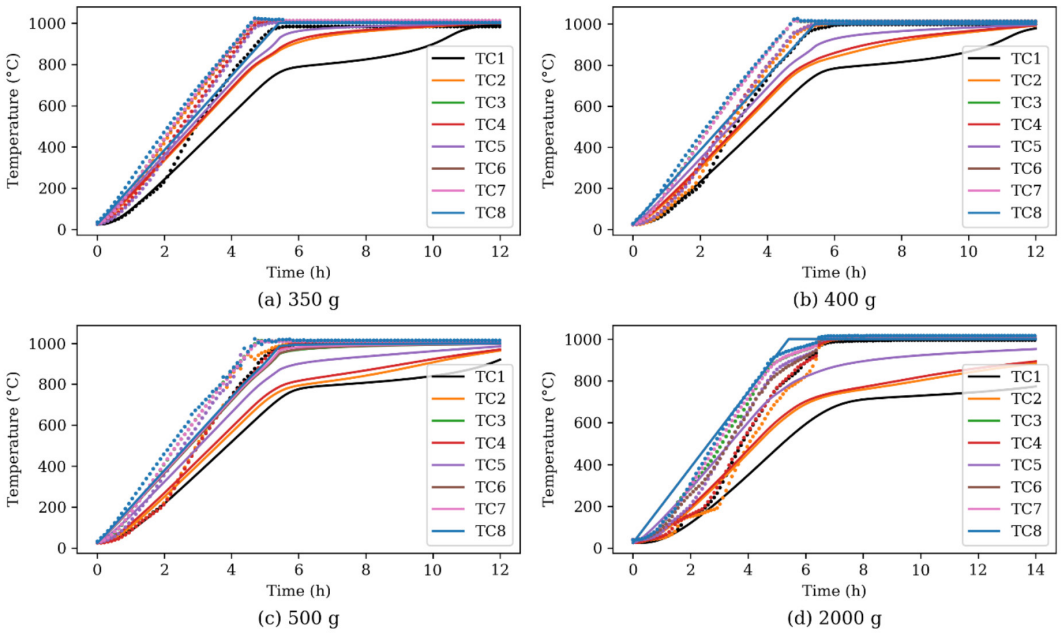

Figure 4—Experimental and model temperature profiles for (a) 350 g; (b) 400 g; (c) 500 g; (d) 2000 g, where dotted lines indicate experimental data and solid lines indicate the mode

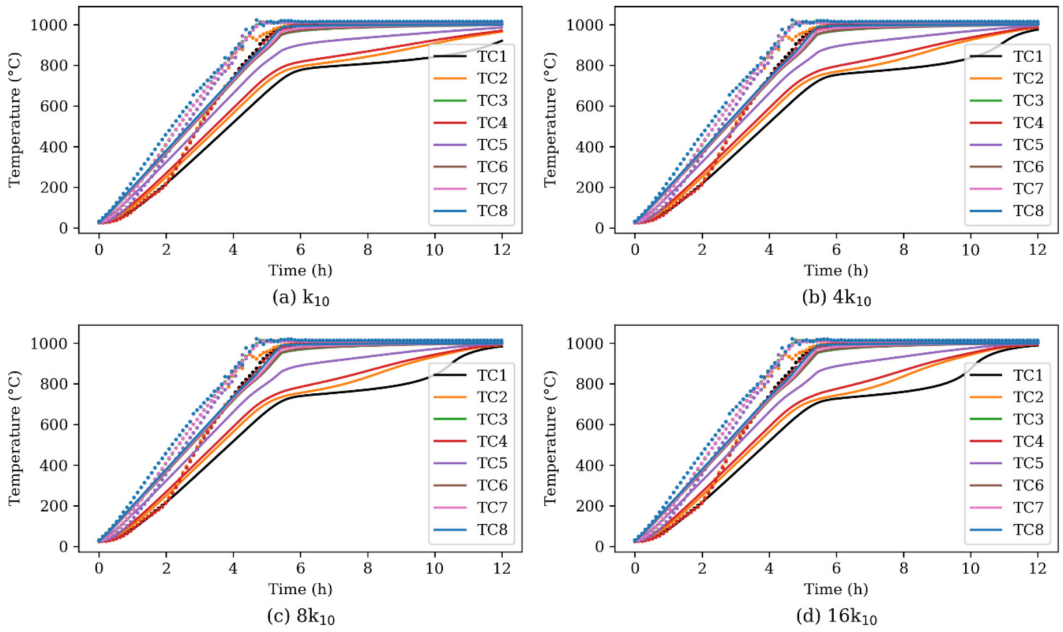

Figure 5—Effect of increasing pre-exponential factor for (a) k_{10}; (b) $4k_{10}$; (c) $8k_{10}$; (d) $16k_{10}$, where dotted lines indicate experimental data

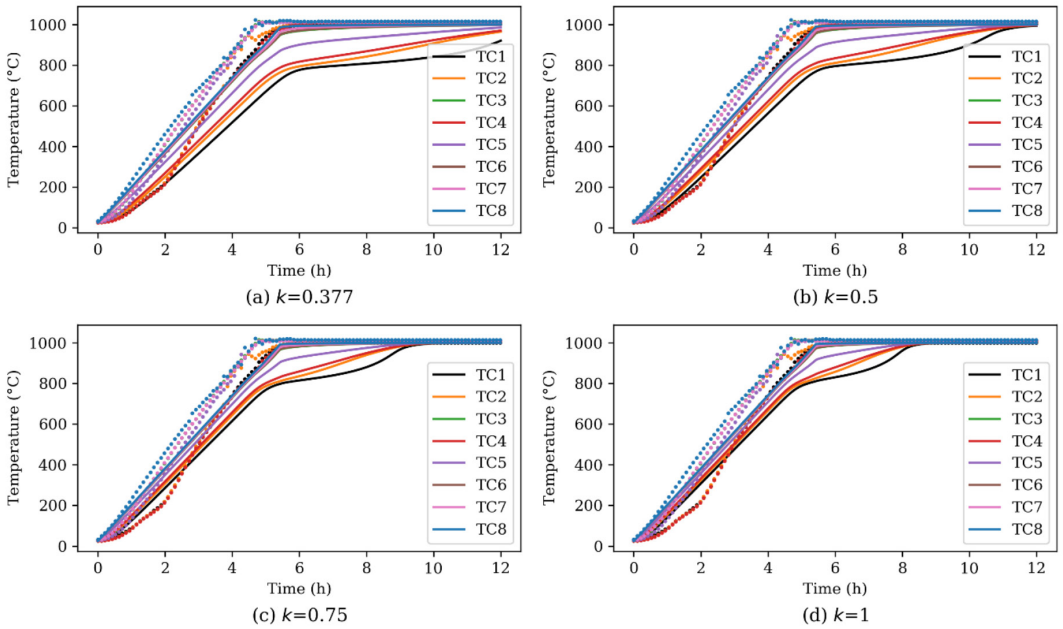

Figure 6—Effect of increasing (constant) thermal conductivity for (a) k = 0:377; (b) k = 0:5; (c) k = 0:75; (d) k = 1, where dotted lines indicate experimental data

It should be noted, however, that a constant value for k is not necessarily an accurate representation, hence Figure 7 depicts the effects of varying the thermal conductivity of the system linearly with temperature as per Equation [26] (although Laubitz (1959) shows that powders can vary logarithmically or exponentially depending on the powder composition). Equation [26] is derived on the basis that k can be assumed to be equal to 0.377 W m^{-1} K^{-1} at 25°C and 1 W m^{-1} K^{-1} at 1000°C.

$$k(T) = 6.39\times10^{-4}T + 0.1865 \quad [26]$$

The presented adjustments to the model achieve conservative results, which is useful in industrial practice, although there is still some inaccuracy. It is possible that there exists a convective contribution to heat transfer within the vessel, but more work is required to investigate this. Furthermore, it would be beneficial to investigate whether the heat transfer limitations have a greater effect on experiments conducted in larger vessels with larger masses, as it is clear from the data obtained that, at the scale and heating rate tested, the heat transfer limitations are not pronounced.

Proposed tunnel kiln optimization

The model can also be used to perform a sensitivity analysis to

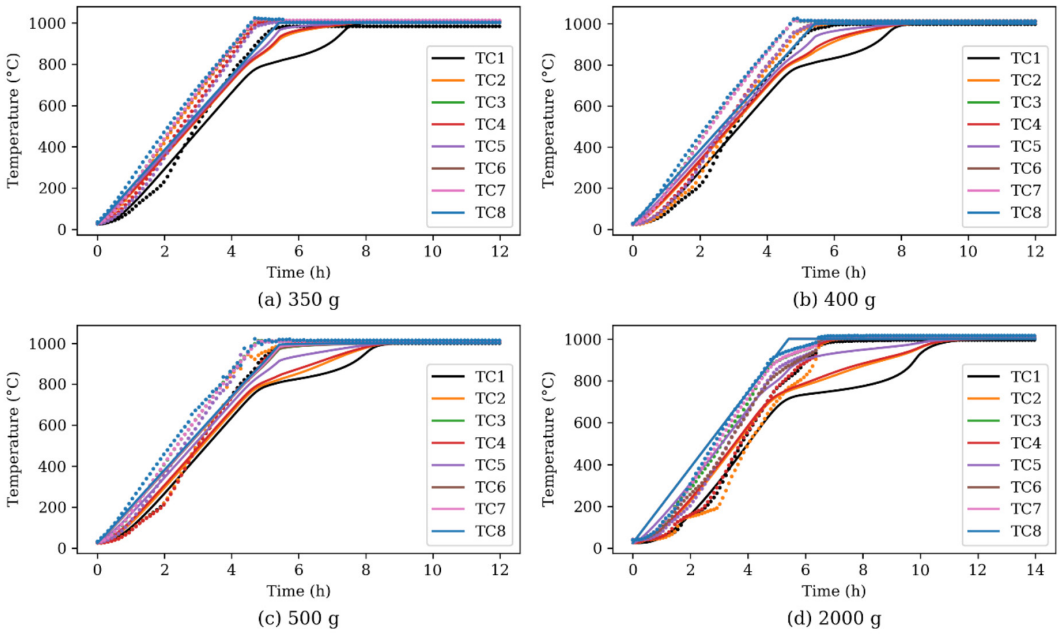

Figure 7—Experimental and model temperature profiles with a linearly increasing k, for (a) 350 g; (b) 400 g; (c) 500 g; (d) 2000 g, where dotted lines indicate experimental data

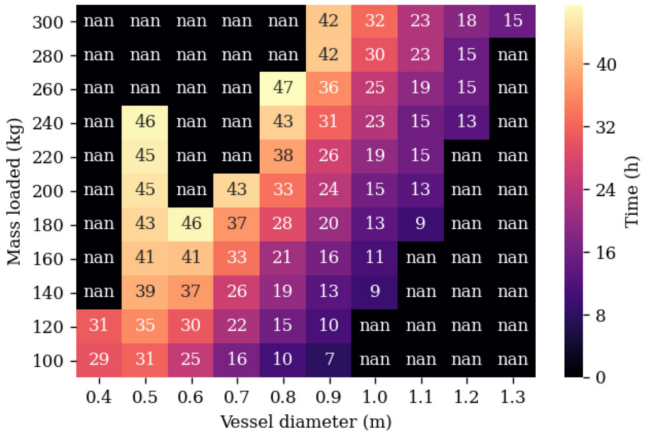

Figure 8—Time to reach final temperature, where 'nan' indicates a null value due to an unsuitable configuration or a centre point not having reached 950°C

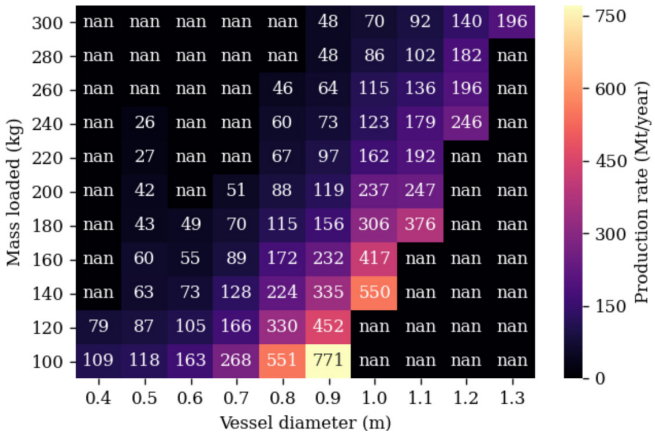

Figure 9—Material processing rate, where 'an' indicates a null value due to an unsuitable configuration or a centre point not having reached 950°C

predict the effect of vessel size on any given mass. A range of different cases with different masses (100–300 kg) and vessel diameters (0.4–1.4 m), using the model with a linearly varying thermal conductivity term and a heating rate of 10°C min^{-1}, was simulated over 48 hours. This sensitivity analysis was used to see which configurations achieved at least 950°C (when the reactions will be virtually completed) within the 48 hours and how long it took. This is depicted in Figure 8, and as can be expected, a shallower material bed tends to achieve temperature faster (with the height sometimes preventing temperature being reached at all).

Unrealistically tall vessels, and unsuitably thin material beds were not included and are represented by a 'nan' term in the figures (with acceptable heights falling within 20–300% of the vessel diameter). Shallow beds were not included as this analysis is limited to cylindrical vessels, and a configuration where material heating is primarily dominated by the top layer would be better suited to a cubic/rectangular loading (as the mass loading can be 21.5% greater). The upper limit of the height of vessels and their loading was set to a factor of three vessel diameters for structural stability reasons.

Using several patents for the direct reduction of iron in a tunnel kiln as a guide, the dimensions for a hypothetical tunnel kiln have been set as 4 m × 4 m ×100 m ($W \times H \times L$) (Hauxing, 2014; Qingfeng, 2005; Xinzheng, 2020; Yicheng, 2014; Zhongji, 2012). This can be used to estimate a material processing rate. Given the time required to reach 950°C, the residence time in the furnace (with interest limited to the heating and holding at temperature only and not cooling) can be calculated and used to estimate a product throughput for each configuration assuming full conversion. Full conversion in this context implies a feed of pure reactants converting fully to products (with additional excess

carbon) whereby 1 kg feed yields approximately 0.47 kg product. It should be noted that the number of vessels is maximized for each configuration by stacking multiple layers on top of each other and side by side. Additionally, only 80% of the available area was utilized to allow for sufficient space between vessels and the walls/roof and consecutive kiln cars.

As per Figure 9, the optimum is a shallow bed (on the edge of the imposed limit on bed height) and a production rate of 771 Mt/a is predicted. This value is a bit large, with direct iron reduction tunnel kilns processing between 100–500 Mt/a (Qingfeng, 2005), but could be achievable. Naturally, at this point of development of suitable technology, these calculations should be deemed as indicative only and should eventually be confirmed by practical results. However, the indications can be used for initial techno-economic assessments to determine if it is worthwhile to invest further in scaling up the technology.

Conclusions

The model presented describes the heat transfer within a reacting bed of gypsum and coal by means of a two-dimensional transient finite difference method.

The model achieves reasonable results and matches the trends observed in experimental work well. However, it is still recommended that larger scale experiments be conducted as the model shows an increasing inaccuracy as the mass and vessel diameter is increased.

A sensitivity analysis for a hypothetical tunnel kiln was used to determine the optimum cylindrical vessel configuration to maximize the possible material processing rate. The analysis found that a shallower material bed results in a more optimal set-up, with more efficient heat transfer. This results in an estimated production rate of 771 Mt/a. Although an actual achievable production rate will only be known once a full-scale plant has been built and operated, the predictions are deemed sufficient to decide whether to further invest in the development of the technology.

The model has good flexibility and can be updated and improved readily. The model shows good suitability for the prediction of the heat transfer within a reacting bed of solid gypsum and coal.

Acknowledgements

The author would like to extend thanks to the Department of Trade, Industry and Competition of South Africa for sponsoring the project, ROC Water for their part in managing the project, and Foskor for making phosphogypsum available for use for the experiments.

References

Akah, A. 2017. Application of rare earths in fluid catalytic cracking: A review. *Journal of Rare Earths*, vol. 35. p. 941.

De Beer, M., Maree, J.P., Liebenberg, L., and Doucet, F.J. 2014. Conversion of calcium sulphide to calci-um carbonate during the process of recovery of elemental sulphur from gypsum waste. *Waste Management*, vol. 34, no. 11. pp. 2373–2381.

De Beer, M., Doucet, F.J., Maree, .P., and Liebenberg, L. 2015. Synthesis of high-purity precipitated calcium carbonate during the process of recovery of elemental sulphur from gypsum waste. *Waste Management*, vol. 46. pp. 619–627.

Bejan, A. 2013. Convection Heat Transfer. 4th edn. Wiley.

Brooks, M.W. ánd Lynn, S. 1997. Recovery of calcium carbonate and hydrogen sulfide from waste calcium sulphide. *Industrial & Engineering Chemistry Research*, vol. 36. pp. 4236–4242.

Çengel, Y.A. and Ghajar, A.J. 2015. Heat and Mass Transfer: Fundamentals & Applications. 5th edn. McGraw-Hill, New York.

Cork, D.J., Jerger, D.E., and Maka, A. 1986. Biocatalytic production of sulphur from process waste streams. *Biotechnology and Bioengineering*, vol. 16. pp. 149–162.

Dutta, T., Kim, K.H., Uchimiya, M., Kwon, E.E., Jeon, B.H., Deep, A., and Yun, S.T. 2016. Global demand for rare earth resource and strategies for green mining. *Environmental Research*, vol. 150. pp. 182–190.

Engineering ToolBox. 2003. Specific heat of solids. https://www.engineeringtoolbox.com/specific-heat-solids-d_154.html

Finney, K.N., Sharifi, V.N., and Swithenbank, J. 2009. Fuel pelletization with a binder: Part II-the impacts of binders on the combustion of spent mushroom compost-coal tailing pellets. *Energy & Fuel*, vol. 23. pp. 3203–3210.

Godbee, H.W. and Ziegler, W.T. 1996. Thermal cConductivities of MgO, Al_2O_3, and ZrO_2 Powders to 850°C. *Journal of Applied Physics*, vol. 37, no. 1. pp. 40–55.

Gorkan, A.N., Prada, S.D., Pathak, G., and ,, S.S. 2000. Vanadium catalysed gasification of carbon and its application in the carbothermic reduction of barite. *Fuel*, vol. 79. pp. 821–827.

Green, D.W. and Perry, R.H. 2008. Perry's Chemical Engineers' Handbook. 8th edn. McGraw-Hill, New York.

Hauxing, J. 2014. Chinese patent no. CN203534155U.

Jagtap, S.B., Pande, A.R., and Gokarn, A.N. 1990. Effect of catalysts on the kinetics of the reduction of barite by carbon. *Industrial & Engineering Chemistry Research*, vol. 29. pp. 795–799.

Kale, B.B., Pande, A.R., and Gokarn, A.N. 1992. Studies in the carbothermic reduction of phosphogypsum. *Metallurgical and Materials Transactions B*, vol. 23. p. 567.

Kato, T., Murakami, K., and Sugawara, K. 2012. Carbon reduction of gypsum produced from flue gas desulfurization. *Chemical Engineering Transactions*, vol. 29. pp. 805–810.

Kulczycka, J., Kawaski, Z., Smol, M., and Wirth, H. 2016. Evaluation of the recovery of rare earth elements (REE) from phosphogypsum waste-case study of the WIZOW chemical plant (Poland). *Journal of Cleaner Production*, vol. 113. pp. 345–354.

Laubitz, M. 1959. Thermal conductivity of powders. *Canadian Journal of Physics*, vol. 37. pp. 798–808.

Li, H.J. and Zhuang, Y.H. 1999. Catalytic reduction of calcium sulfate to calcium sulfide by carbon monoxide. *Industrial & Engineering Chemistry Research*, vol. 38, no. 9. pp. 3333–3337.

Luikov, A., Shashkov, A., Vasilievv, L., and Fraiman, Y. 1968. Thermal conductivity of porous systems. *International Journal of Heat and Mass Transfer*, vol. 11. pp. 117–140.

Ma, L., Niu, X., Hou, J., Zheng, S., and Xu, W. 2011. Reaction mechanism and influence factors analysis for calcium sulfide generation in the process of phosphogypsum decomposition. *Thermochimica Acta*, vol. 526. pp. 163–168.

Mark, H.F., Othmer, D.F., Overberger, C.G., and Seaborg, G.T. 1978. *Kirk-Othmer: Encyclopedia of Chemical Technology*. 3rd edn. Wiley-Interscience, New York.

Mbhele, N.R., van der Merwe, W., Maree, J.P., and Theron, D. 2009. Recovery of sulphur from waste gypsum. *Proceedings of the International Mine Water Conference*, Pretoria, South Africa, 19-23 October 2009. https://www.imwa.info/docs/imwa_2009/IMWA2009_Mbhele.pdf

Miao, Z., Yang, H., Wu, Y., Zhang, H., and Zhang, X. 2012. Experimental studies on decomposing properties of desulfurization gypsum in a thermogravimetric analyzer and multi-atmosphere fluidized beds. *Industrial & Engineering Chemistry Research*, vol. 51. pp. 5419–5423.

Motaung, S., Zvimba, J.N., Maree, J.P., and Kolesnikov, A. 2015. Thermochemical reduction of pelletized gypsum mixed with carbonaceous reductants. *Water* SA, vol. 41. pp. 369.

Nengovhela, N.R., Strydom, C.A., Maree, J.P., Oosthuizen, S., and Theron, D.J. 2007. Recovery of sulphur and calcium carbonate from waste gypsum. *Water* SA, vol. 33. pp. 741–747.

Ning, P., Zheng, S.C., Ma, L.P., Du, Y.L., Zhang, W., Niu, X.K., and Wang, F.Y. 2011. Kinetics and thermodynamics studies on the decomposition of phosphogypsum in different atmospheres. *Advanced Materials Research*, vol. 160. pp. 842–848.

Oates, J.A.H. 1986. Lime and Limestone: *Chemistry and Technology*, Production and Uses. Wiley-VCH, Weinheim.

Oberholzer, J.J. and Nel, S.S. 2020. Analytical report: Ash and coal samples. UIS Analytical Services, Pretoria.

Oh, J.S. and Wheelock, T.D. 1990. Reductive decomposition of calcium sulphate with carbon monoxide: reaction mechanism. *Industrial & Engineering Chemistry Research*, vol. 29. pp. 544–550.

Qingfeng, Y. 2005. Tunnel kiln without exterior combustion chamber and production of direct reduced iron by composite tunnel kiln. Chinese patent no. CN1804049A.

Roine, A. 2018. HSC Chemistry. Outotec, Pori. http://www.outotec.com/HSC

Ruto, S., Maree, J.P., Zvinowanda, C.M., Louw, W.J., and Kolesnikov, A.V. 2011. Thermal studies on gypsum in a pilot-scale, rotary kiln. *Proceedings of Water in the South African Minerals Industry*. Southern African Institute of Mining and Metallurgy, Johannesburg. pp. 15–17.

Selim, H., Gupta, A.K., and Al Shoaibi, A. 2013. Effect of reaction parameters on the quality of captured sulphur in Claus process. *Applied Energy*, vol. 104. pp. 772–776.

Sliger, A.G. 1988. The MW Kellogg Company KEL-S Process. *Proceedings of the Second International Symposium on Phosphogypsum*, Miami, Florida. Florida Institute of Phosphate Research. pp. 89–107.

Strydom, C.A., Groenewald, E.M., and Potgieter, J.H. 1997a. Thermogravimetric studies of the synthesis of CaS from gypsum, $CaSO_42H_2O$ and phosphogypsum. *Journal of thermal analysis*. vol. 49, no. 3. pp. 1501.

Strydom, C.A., Groenewald, E.M. and Potgieter, J.H. 1997b. Thermogravimetric studies of the synthesis of CaS from gypsum, $CaSO_42H_2O$ and phosphogypsum. *Journal of thermal analysis*, vol. 49, no. 3. p. 1501.

Tao, D., Chen, S., Parekh, B.K., and Hepworth, M.T. 2001. An investigation of a thermochemical process for conversion of gypsum and pyrite wastes into useful products. *Advances in Environmental Research*, vol. 5. pp. 277–284.

Tesárek, P., Drchalová, J., Kolísko, J., Rovnaníková, P., and Černý, R. 2007. Flue gas desulfurization gypsum: Study of basic mechanical, hydric and thermal properties. *Construction and Building Materials*, vol. 21, no. 7. pp. 1500–1509.

Trikkel, A. and Kuusik, R. 1994. Tallinna tehnikaulik. *Toimi*, vol. 45. pp. 742.

Van Vuuren, D. and Maree, J. 2018. A novel process to recover sulfur, lime and rare earths from gypsum. Department of Chemical Engineering, University of Pretoria.

Walawalkar, M., Nichol, C.K., and Azimi, G. 2016. *Process investigation of the acid leaching of rare earth elements from phosphoogypsum using HCl, HNO_3 and H_2SO_4*. http://dx.doi.org/10.1016/j.hydromet.2016.06.808

Welty, J.R., Wicks, C.E., and Wilson, R.E. 1969. *Fundamentals of Momentum*, Heat, and Mass Transfer. 5th edn. Wiley. New York.

Windholz, M. 1983. The Merck Index. 10th edn. Merck & Co., Inc, New Jersey.

Xinzheng, B. 2020. Chinese patent no. *CN111359544A*.

Yan, B., Ma, L., Ma, J., Zi, M., and Yan, X. 2014. Mechanism analysis of CaS transformation in -phosphogypsum decomposition with Fe catalyst. *Industrial & Engineering Chemistry Research*, vol. 53. pp. 7648–7654.

Yicheng, F. 2014. Chinese patent no. Wo2014169442A1.

Yunusova, S.S. 2004. Composite wall materials and products based on phosphogypsum, obtained by semi-dry pressing. Samara State Architecture Academy.

Zadick, T.W., Zavaleta, R., and McCandless, F.P. 1972. Catalytic reduction of calcium sulfate to calcium sulfide with carbon monoxide. *Industrial & Engineering Chemistry Research*, vol. 11. pp. 283.

Zhang, W., Li, X., Qu, Z., Zhao, Q., and Chen, G. 2010a. Facile solution synthesis and characterization of $CaCO_3$ microspheres with urchin-shaped structure. *Material Letters*. vol. 64. pp. 71–73.

Zhang, W., Li, X., Qu, Z., Zhao, Q., and Chen, G. 2010b. Facile solution synthesis and characterization of $CaCO_3$ microspheres with urchin-shaped structure. *Materials Letters*, vol. 64. pp. 71–73.

Zhongji, H. 2012. Chinese patent no. CN102643944A. ◆